Acta Materialia 154 (2018) 228–236

Contents lists available at ScienceDirect

Acta Materialia

journal homepage: www.elsevier.com/locate/actamat

Full length article

Simple model for particle phase transformation kinetics

Raphael M.C.V. Reis [a, *], Edgar D. Zanotto [b]

[a] Department of Metallurgical and Materials Engineering (VMT), Fluminense Federal University (UFF), Av. dos Trabalhadores, 420, 27255-125, Volta Redonda, RJ, Brazil
[b] Vitreous Materials Laboratory (LaMaV), Department of Materials Engineering (DEMa), Federal University of São Carlos (UFSCar), Rod. Washington Luís, km. 235, 13565-905, São Carlos, SP, Brazil

ARTICLE INFO

Article history:
Received 23 March 2018
Received in revised form
17 May 2018
Accepted 17 May 2018
Available online 19 May 2018

Keywords:
Phase transformation
Kinetics
Differential scanning calorimetry (DSC)
Crystallization
Glass

ABSTRACT

We propose a new model for the kinetics of phase transformation of particles starting from surface and internal nucleation sites. The model's analytical equation is very simple, allowing for easy usage and interpretation. We tested the model against the crystallization of glass particles using differential scanning calorimetry, DSC. We used diopside ($CaO{\cdot}MgO{\cdot}2SiO_2$) glass particles having different number densities of surface nucleation sites, N_S, and also lithium disilicate glass particles, which show simultaneous surface and internal crystallization, having different number densities of internal nuclei, N_V. Simulations of DSC traces provided accurate predictions of the transformation kinetics. We compared our model results to those of rigorous (more complex) models in terms of three non-dimensional parameters: the number of surface nuclei, the number of internal nuclei and a non-dimensional time. Our model, with a simpler equation, provided similar results. We believe it may also provide a more realistic approximation for particles that sinter during phase transformation, such as glass particles that simultaneously crystallize during sintering, and for transformations starting from the grain boundaries in polycrystalline materials.

1. Introduction

Phase transformations are a central phenomenon in materials science and engineering and several models have been proposed, which are routinely employed to interpret or predict their kinetics. The Johnson-Mehl-Avrami-Kolmogorov (JMAK) theory [1–5] is one of the most used. It considers a transformation process in an infinite n-dimensional space from randomly dispersed sites. In its general form, Eq. (1), the transformed fraction, α, is calculated from the extended volume, α', which is an expression for the growth of grains or crystals of the new phase without considering their impingement. This equation has been used extensively to study the kinetics of phase transformations via nucleation and growth in many materials, including glass and polymer crystallization.

$$\alpha = 1 - \exp(-\alpha') \quad (1)$$

Care must be taken not to violate the model's assumptions [6]. For example, when a certain transformation starts from particle surfaces and grain boundaries, the calculation of the transformed fraction demands an expression that considers the non-uniform dispersion of the nuclei. Samples of finite size also demand an adequate approach [7]. Other models have been crafted ignoring these assumptions but may still be reasonable approximations [8,9].

Sintering with concurrent crystallization of glass particles is a particular interesting and commercially important case. Crystallization invariably starts from heterogeneous nucleation on particle surfaces, but may also happen from internal nucleation, and controlling the crystallization process is essential for optimization of glass-ceramics properties and applications [10].

Thirty years ago, Müller proposed a model in which regularly spaced cubic crystals grow from the surface of cubic glass particles [11]. In spite of the model simplicity, it provides useful insights into the transition from 3D to 1D crystal growth due to the coalescence of surface crystals. Once a fully crystalline layer is formed, the crystals can only grow in one direction, *i.e.*, towards the particle's center.

Weinberg also proposed a model for surface and bulk crystallization of spherical particles that conforms to the finite sample size limitation [12]. Villa and Rios discussed the limitations of applying

* Corresponding author.
E-mail address: raphaelmreis@gmail.com (R.M.C.V. Reis).

https://doi.org/10.1016/j.actamat.2018.05.039
1359-6454/

the JMAK model to samples of finite size and proposed a rigorous mathematical model to describe the surface and volumetric transformation of particles of different shapes [13]. However, the Weinberg and Villa-Rios models are mathematically complex, requiring a numerical solution, thus making it more difficult to use.

In this article, we propose a new model to describe the phase transformation kinetics from nucleation sites on the surface and in the interior of particles, described in Section 3.1. The model equation is very simple, allowing for easy usage and interpretation of results. We tested it using differential scanning calorimetry, DSC, of glass particles. In Section 3.2.1, we test the model for surface crystallization from a finite number of nuclei using spherical diopside glass particles. In Section 3.2.2, we use lithium disilicate glass particles to evaluate the model against a simultaneous surface and internal crystallization. We critically discuss these results in Section 4.1. In Section 4.2, we discuss our model using three non-dimensional parameters: the number of surface nuclei, the number of internal nuclei and a non-dimensional time. This parameterization is used in Section 4.3 to compare our model to the complex models proposed by Weinberg, as well as Villa and Rios. With a much simpler, analytical equation, our model provides similar results to those of the rigorous models. Moreover, it may provide more realistic transformation kinetics for cases where the particles sinter prior or simultaneously to the phase transformation, for instance in glass sintering and DSC analysis of glass particles. This new model could also be used for transformations starting from grain boundaries in polycrystalline materials.

2. Experimental

We tested our model using the crystallization peak from differential scanning calorimetry (DSC) analysis of powdered (micron size) and millimetric glass samples.

2.1. Glass preparation

We used two glasses that undergo stoichiometric crystallization, *i.e.*, the crystalline phase has the same composition as the parent glass. Diopside glass, $MgO{\cdot}CaO{\cdot}2SiO_2$, shows only surface nucleation, whereas lithium disilicate, $Li_2O{\cdot}2SiO_2$, presents both surface and volumetric crystallization. We produced both glasses by melting high purity raw materials in a platinum crucible in an electrical furnace followed by quenching by pouring the melt on a steel plate. The details of this process have been reported elsewhere [14,15].

A powder consisting of diopside glass spherical particles was produced [15]. The particle size distribution was determined by automated image analysis of approximately 18,000 particles using an ImageJ [16] macro. The powder has a narrow particle size distribution, with approximately 90% of the particles between 50 and 100 μm, with $d_{50} = 76\ \mu m$. The lithium disilicate glass was cut to millimetric cubic samples using a diamond wafering blade.

2.2. Differential scanning calorimetry

The differential scanning calorimetry (DSC) experiments were performed in a DSC 404 – NETZSCH using a 10 °C/min heating rate. Prior to each run, a baseline was acquired with empty crucibles.

2.2.1. Diopside glass

Two samples of spherical diopside glass powders were analyzed. The samples weighed approximately 30 mg and differed by their density of surface nucleation sites, N_S. To increase the value of N_S, we seeded the particle surfaces with a crystalline diopside powder. The crystalline powder was obtained by heat treating a piece of diopside glass at 1200 °C for several hours, grinding it with a mortar and pestle and sieving it through a 22 μm nylon mesh. The crystalline powder was then mixed with ethanol (1:1 by mass) and a couple of drops of the suspension were dropped on the glass powder in the DSC crucible. Approximately 13 mg of crystalline diopside was added to the glassy powder.

2.2.2. L2S glass

Four cubic samples of L2S glass were analyzed: one with 1.515 mm and three others with 2.46 mm. Two of the 2.46 mm samples were subjected to a nucleation heat treatment to increase the number of internal nucleation sites, N_V. One sample was treated for approximately 18 min (N_{V1}) and another for 56 min (N_{V2}), both at 480 °C. The two other samples were not subjected to a nucleation step (N_{V0}).

The number of nuclei per unit volume, N_V , was determined by optical microscopy. One sample for each condition (N_{V0}, N_{V1} and N_{V2}), with sides of approximately 3 mm × 3 mm and thickness of 1 mm were heat treated in the DSC furnace for 5 min at 600 °C to develop the nuclei to observable sizes. The samples were polished to remove the surface crystalline layer. Transmitted light microscopy with cross polarizers was used to take images at different focus heights, encompassing the whole sample thickness (0.83 mm after polishing). The crystals were counted for each sample, and N_V was finally determined by dividing the number of crystals by the sampled volume (area of the micrograph x 0.83 mm).

2.3. Simulation and fitting

We used the software PTC – Mathcad 13 for curve simulation and ORIGINLAB – Origin 8.5 for data treatment and curve fitting.

For diopside glass, we used a 2nd degree polynomial for $\log(U)$ to fit data measured for this glass batch [17]. Eq. (2) describes the data very well from 1000 to 1250 K.

$$\log(U) = -64.705 + 0.07312\,T - 2.063 \times 10^{-5}\,T^2,\ T(K),\ U(m/s) \quad (2)$$

For L2S we used a 2nd degree polynomial for $\log(U)$ fit to data measured for this glass batch from 838 to 983 K [18]. Eq. (3) adequately describes literature data [19] for temperatures as low as 713 K ($T_g \sim 727$ K).

$$\log(U) = -57.912 + 0.09325\,T - 4.0844 \times 10^{-5}\,T^2,\ T(K),\ U(m/s) \quad (3)$$

We simulate the DSC crystallization peaks by taking the temperature derivative of the transformed fraction, Eq. (4). We assume the crystallization of a single phase of constant crystallization enthalpy, and that $U(T)$ is independent of the transformed fraction.

$$DSC(T) = \frac{d\alpha(T)}{dT} \quad (4)$$

To compare with the simulations, a sigmoidal baseline was adjusted and subtracted from the experimental peaks. The peak area was normalized to unity [18].

3. Results

3.1. The current model

3.1.1. Surface transformation from a finite number of nuclei: conical model

First, we consider the tridimensional transformation from a

finite number of surface nuclei, N_S, towards the center of a spherical particle. We assume that the nuclei are randomly dispersed on the particle's surface and that their number remains fixed during the whole process. This is a reasonable assumption for many experimental conditions [8,9], although it does not always hold [20].

If the transformation starts simultaneously from all points of the particle surface, a full transformed layer grows, as shown in Fig. 1 (a). The volume contraction model, or Jander's law [21], Eq. (5), gives the transformed fraction for the case of an infinite N_S.

$$\alpha^S(t) = 1 - \left(1 - \frac{h(t)}{R}\right)^3 \tag{5}$$

where $h(t)$ is the transformed length in time t and R is the particle radius. This equation is valid up to the time needed for the layer to reach the center of the particle, *i.e.*, when $h(t) = R$. For an isothermal heat treatment, $h(t) = U \cdot t$, where U is the transformation rate at a given temperature. More generally, when the temperature changes with time, we can write:

$$h(t) = \int_{t0}^{t} U(t)dt \tag{6}$$

Any suitable expression for $T(t)$ may be used with Eq. (6) to describe the thermal path. For a constant heating rate, q, as we used in the DSC simulations, h is given by Eq. (7).

$$h(T) = \int_{T0}^{T} \frac{U(T)}{q} dT \tag{7}$$

When a surface transformation starts from a finite N_S, the surface is gradually transformed, Fig. 1 (b). The impingement-corrected 2D transformation kinetics of randomly dispersed circular regions on an infinite surface is given by Eq. (8).

$$\alpha_{2D}(t) = 1 - \exp\left(-\pi \cdot N_S \cdot h(t)^2\right) \tag{8}$$

The subscript *2D* is used to denote the transformed 2D fraction of the particle surface. Complete surface transformation is asymptotically approached due to the assumption of infinite 2D space populated by randomly dispersed nuclei. In a finite size particle, however, 100% transformation can be achieved, as long as there is at least one nucleus on the particle's surface.

The tridimensional transformed fraction of a particle from its surface can be approximated by the product of the "full-layer mechanism", Eq. (5), and the fractional 2D surface occupation from a finite number of nuclei, Eq. (8).

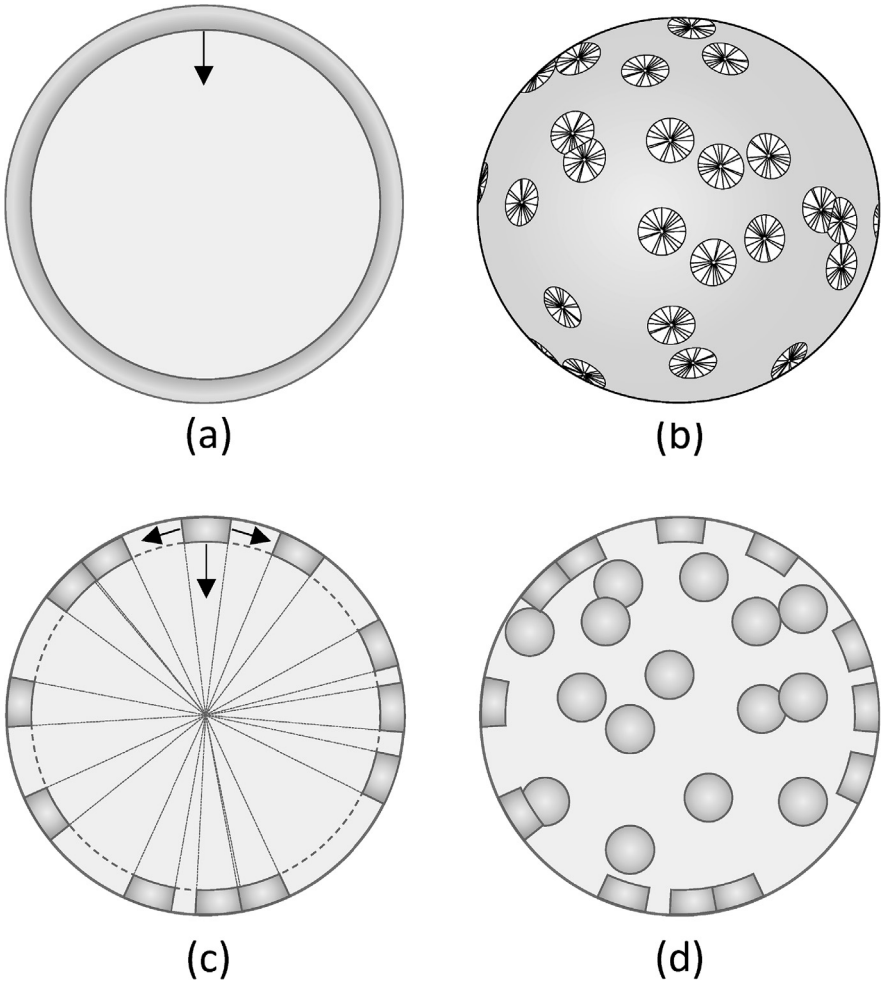

Fig. 1. Different transformation kinetics of spherical particles. (a) Transformation of a surface layer. (b) 2D Surface growth. (c) Volumetric transformation from a finite number of surface sites and (d) from surface and internal sites.

$$\alpha^S(t) = \left(1 - \left(1 - \frac{h(t)}{R}\right)^3\right) \cdot \left(1 - \exp\left(-\pi \cdot N_S \cdot h(t)^2\right)\right) \quad (9)$$

Eq. (9) describes the transformation with the shape of a cone truncated by two spheres – the particle surface and the hypothetical full layer, Fig. 1 (c). Although no reports of transformation with this geometry is known to us, we show in Section 4.3 that this is a good approximation for the semi-spherical shape. There is no explicit limitation of using Eq. (5) to other isometric particle geometries; hence Eq. (9) should be the same for a cubic particle.

Eq. (9) is valid for $h(t) \leq R$. This limitation is only important when the number of nuclei is very low, in which case α_{2D} does not reach ~ 1 before the transformed layer reaches the particle center. We demonstrate in Section 4.2 that this issue is not relevant if the particle has more than 10 surface nuclei. The model can be extended to longer times by considering $h = R$ only in the first term of Eq. (9) for times when $h(t) > R$; Eq. (9) then reduces to Eq. (8). This approximation enables us to compute the phase transformation kinetics up to full transformation of the sample. The transformation is arrested in the direction of the particle's radius but may still take place laterally.

3.1.2. Simultaneous surface and volume transformation

Some materials undergo both surface and volume transformation, as schematically shown in Fig. 1 (d). Here we consider the transformation due to a fixed number of randomly distributed internal nuclei, given by Eq. (10). This equation does not take the finite particle size into account, but other expressions can be used for the transformation due to internal nuclei.

$$\alpha^V(t) = 1 - \exp\left(-\frac{4}{3}\pi \cdot N_V \cdot h(t)^3\right) \quad (10)$$

Levine et al. proposed models for the transformation of particles starting from internal nuclei for different conditions [7]. As an example, for a fixed number of internal nuclei, they propose Eq. (11).

$$\alpha^V(t) = 1 - \exp\left(-N \cdot \left(\left(\frac{h(t)}{R}\right)^3 - \frac{9}{16}\left(\frac{h(t)}{R}\right)^4 + \frac{m}{32}\left(\frac{h(t)}{R}\right)^6\right)\right), \quad m = \max(5{,}26 - 0{,}26N, 1) \quad (11)$$

where N is the number of crystals in each particle and m is a correction function that depends on the number of crystals. Interestingly, without their correction function, *i.e.*, using $m = 1$, it can be shown that this equation gives a very good approximation to the Villa-Rios model [13] for the transformation from internal nuclei (see Section 4.3.3). In this case, however, N is not the *exact* number of crystals per particle, it is instead the *average* number of crystals per particle.

For a constant nucleation rate, I, the classical impingement-corrected result, Eq. (12), could be used [22].

$$\alpha^V(t) = 1 - \exp\left(-\frac{\pi}{3} I \cdot t \cdot h(t)^3\right) \quad (12)$$

To calculate the total transformed fraction, we start by calculating the remaining unreacted fraction after surface transformation, $1 - \alpha^S$. The remaining fraction should be partially (or totally) transformed due to volumetric transformation, α^V. Therefore, $(1 - \alpha^S) \cdot \alpha^V$ is the extra crystallization due to internal nuclei and $(1 - \alpha^S) \cdot (1 - \alpha^V)$ is the remaining untransformed fraction after surface and volumetric transformation, Eq. (13).

$$1 - \alpha^{S,V} = \left(1 - \alpha^S\right) \cdot \left(1 - \alpha^V\right) \quad (13)$$

Finally, from Equations, (9), (10) and (13), the total transformed fraction is:

$$\alpha^{S,V}(t) = 1 - \left\{1 - \left[1 - \left(1 - \frac{h(t)}{R}\right)^3\right] \cdot \left[1 - \exp\left(-\pi \cdot N_S \cdot h(t)^2\right) \times \right]\right\} \cdot \left[\exp\left(-\frac{4}{3}\pi \cdot N_V \cdot h(t)^3\right)\right] \quad (14)$$

We can also extend the validity of Eq. (14) past $h \leq R$ by making $h = R$ only in the first term of Eq. (14) (Jander's law), as we did in the previous section.

3.2. Tests of the model

3.2.1. Testing for finite number of surface sites: diopside glass

Fig. 2 shows the DSC traces of the original (N_{S0}) and seeded (N_{S1}) spherical diopside powders during heating. The onset of glass transition is detected at approximately 720 °C for both samples. Two exothermic peaks can be seen in both curves, at approximately 900 °C and 1000 °C. The first is due to the crystallization of the glass into diopside and a wollastonite-like phase, while the second peak is the transformation of the wollastonite-like phase to diopside [23]. The two phases show similar growth rates [23].

Seeding the glass particles with a crystalline diopside powder caused a shift of the onset of the glass crystallization peak to lower temperatures, as expected. Both peaks end at similar temperatures. We made a rough estimate of N_{S0} by analyzing the surface of the sintered powder that remained inside the crucible after the DSC run. The surface was covered by impinged crystals, of approximately 10 μm in diameter. The number of crystals per image was divided by the image area resulting in an average value of $N_{S0} = 10^{10} m^{-2}$, with a standard deviation of $2 \times 10^9 m^{-2}$. There is, however, a large uncertainty in this value because only the top surface was analyzed, overlooking the sintered necks and pores in the interior of the sample. It was not possible to estimate N_{S1} due to the presence of the crystallized powder used as a nucleating agent.

Simulations using our model and Eq. (4) describe the change in the crystallization peak shape due to the increase in N_S, as seen in Fig. 3. In the simulations, we used a particle radius of $d_{50}/2 = 38\ \mu m$ and different N_S, as noted in the figure. Simulations

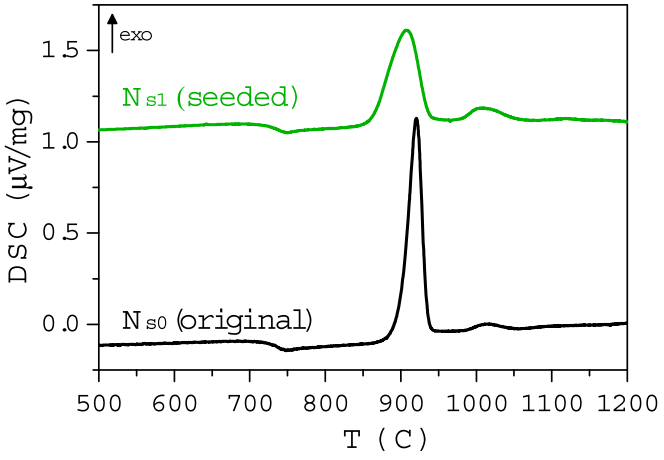

Fig. 2. DSC traces of the seeded and the original diopside-glass powders.

with the measured N_S of $10^{10}m^{-2}$ agrees well with the crystallization peak of the original particles. We also show a simulation made with a value of $3 \times 10^{9}m^{-2}$, which fits the data better. The DSC peak for the N_{S1} sample is similar to the simulated curve with infinite N_S. The beginning of the experimental peak, however, is not as shallow, probably indicating that N_S is still effectively finite. A value of $N_S = 3 \times 10^{11}m^{-2}$ describes the beginning of the crystallization better.

The shoulders of the simulated curves with $N_S = 10^{10}$ and $3 \times 10^{11}m^{-2}$ are due to the change in the transformation dimensionality as a consequence of the finite number of surface nucleation sites. In the early stages, the crystals grow in 3 directions (Fig. 1 (c)) and the crystallization front increases as they grow. When the crystals start to impinge, lateral growth is constrained and crystals can only propagate in 1 direction, toward the particle center (Fig. 1 (a)). The crystallization front area diminishes and, consequently, the transformation rate also decreases. As the temperature increases during a DSC run, the rate of crystallization increases again, due to a higher $U(T)$.

3.2.2. *Testing for simultaneous surface and volume crystallization: L2S glass*

Fig. 4 shows DSC curves for the cubic L2S-glass samples of different values of N_V. We found by microscopy analysis that $N_{V0} = 67$, $N_{V1} = 989$ and $N_{V2} = 2,960$ crystals per mm^3. The onset of glass transition is observed at 454 °C for all samples. As N_V increases, the DSC crystallization peak shifts to lower temperatures, as expected.

For the two N_{V0} samples (1.51 and 2.46 mm), the peak temperature is the same, but the peak for the smaller sample shows a tail at lower temperatures, *i.e.*, the transformation is initially faster than for the larger sample. This is due to the higher influence of surface crystallization for smaller samples, since they have a higher specific surface area.

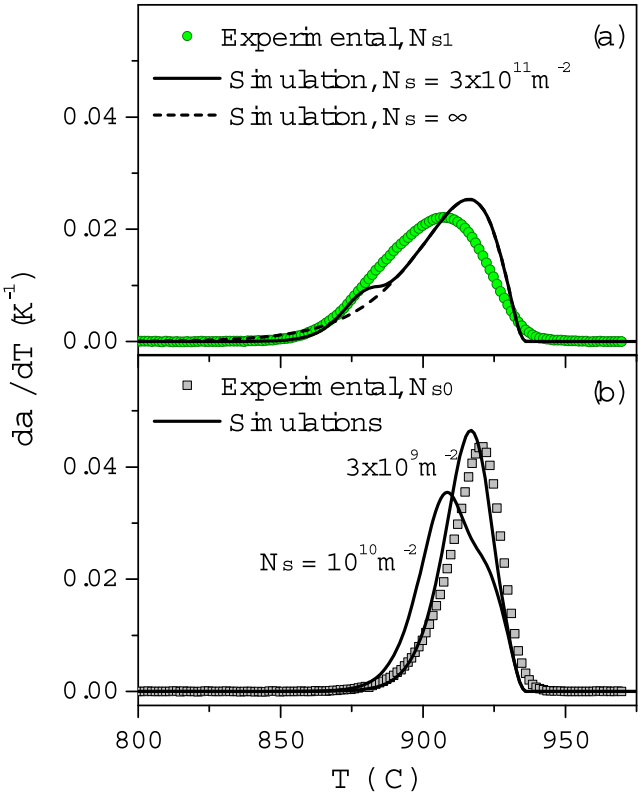

Fig. 3. Crystallization peaks of diopside glass powders of different N_S. (a) Seeded particles, N_{S1}, and (b) original particles, N_{S0}.

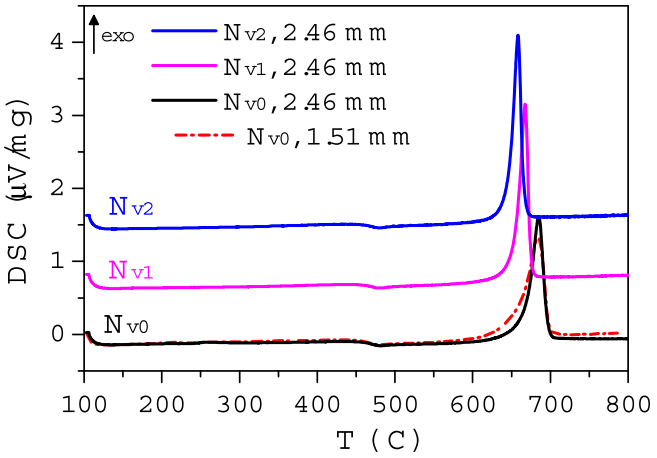

Fig. 4. DSC traces for L2S glass cubes with different numbers of internal nuclei.

Our model captures the increase of the surface contribution to the crystallization peak, for the N_{V0} samples of different sizes, Fig. 5. We performed the simulations considering an infinite number of surface nucleation sites. There is an excellent agreement between the simulated and experimental curves, especially for the 1.51 mm sample. The 2.46 mm simulated curve has a slightly lower peak height (and enlarged peak width) than the experimental result and the peak temperature agrees within 2 °C.

Fig. 6 shows the crystallization peaks for the 2.46 mm cubes with a different number of internal nuclei ($N_{V0} = 67$, $N_{V1} = 989$ and $N_{V2} = 2980$ mm^{-3}). Good agreement is observed for the peak temperatures, within 1 °C for samples N_{V1} and N_{V2}, although peak amplitudes exhibit a poorer fit, perhaps related to a sample-size effect (see Section 4.1).

4. Discussion

In this section, we critically discuss the agreement between the model and experiments and compare the model results to exact (but more complex) models of particle phase transformation.

4.1. *Agreement between simulated and experimental peaks*

Our model captures the effect of the increase in the N_S of

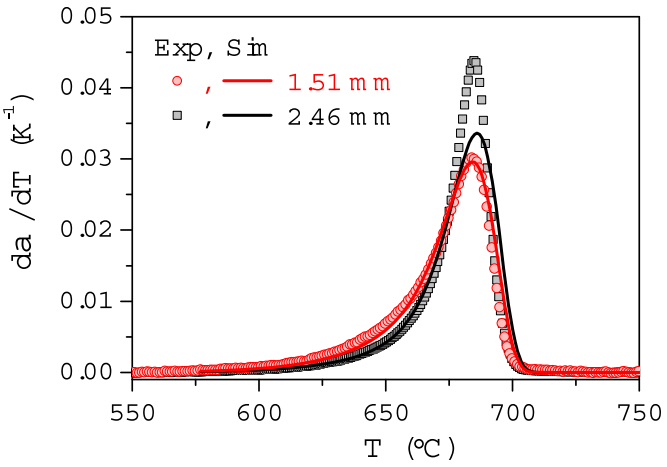

Fig. 5. Crystallization peaks for L2S glass cubes of different sizes and N_{V0}= 67 mm^{-3}.

diopside glass particles. The simulations agree with the shift of about 30 K of the onset of the crystallization peak to lower temperatures and to the increase of about 25 K in peak width observed in Fig. 3.

The interplay between surface and internal crystallization is also well explained by our model. Fig. 7 shows how surface and internal crystallization contributes to the crystallization peak of the 1.51 mm L2S sample. The low temperature peak tail corresponds mainly to surface transformation (dashed curve) while the peak end is directly influenced by the internal transformation (dotted curve). The simultaneous contribution of the two mechanisms (calculated by Eq. (13), full curve) agrees with the experimental data.

We carefully looked into the small discrepancies between the simulated and experimental peaks of Figs. 3–6. We verified that our model simplifications did not have a large impact on the simulations, since the mathematically exact model of Villa and Rios [13] resulted in very similar DSC curves (not shown here) for the parameters of the diopside and L2S samples.

In the calculations of the experimental transformation rates, we assumed that the DSC signal is proportional to the transformation rate, ignoring the effects of heat inertia from the experimental setup and the finite thermal conductivity of the samples [24,25]. Unfortunately, it is not clear how much this effects our data. We see, however, a better agreement for the 1.51 mm L2S sample, which has the smallest mass of all samples (8 mg *vs.* 30–40 mg) and should present the smallest thermal lag.

For the L2S samples, the difference cannot be explained by time dependent crystal nucleation or measurement errors in the crystal growth rates. The crystal nucleation rate is negligible at the peak temperature range [26] and the temperature dependence of crystal growth rate would need to be unrealistically large to explain the misfit. We tested this effect but have not shown it here due to the lack of space.

The crystallization of diopside glass is more complex than we assumed in our simulations, which affects the crystallization peak shape: (i) Diopside glass crystallizes into two different crystalline phases, as explained in Section 3.2. These phases may have different crystallization enthalpies and slightly different crystal growth rates. (ii) Due to the density difference between the glass and the crystalline phases, a void generally appears inside the particles after some degree of crystallization [23], altering the geometry of the transformation. The model also does not consider the

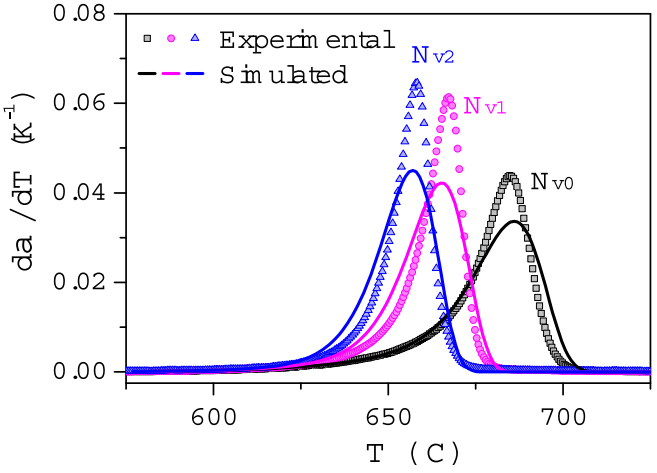

Fig. 6. Experimental and simulated crystallization peaks for 2.46 mm L2S cubes with N_{V0}= 67 mm^{-3}, N_{V1}=989 mm^{-3} and N_{V2}=2980 mm^{-3}.

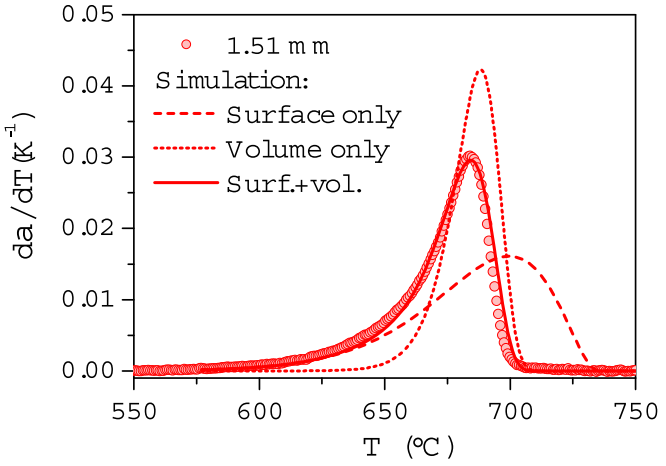

Fig. 7. Experimental crystallization peak for the 1.51 mm L2S glass cube and simulated curves for surface nuclei (dash), internal nuclei (dot), and simultaneous surface and internal crystallization (full curve).

particle size distribution, PSD, the variation of N_S between particles or the change in particle shape due to sintering. For a glass powder with a known PSD, the degree of transformation could be calculated as the volume-fraction-weighted average of the crystallized fraction of each bin of the PSD.

Considering the model deviations from the actual crystallization kinetics of diopside glass and the strong dependence of the transformation rate on the crystal growth rate, we consider the agreement (within one order of magnitude) between the N_S estimated by optical microscopy and the model fitting to be quite good.

4.2. Non-dimensional parameterization

We nondimensionalize our model by defining the parameters of Equations (15)–(17), similarly to the work of other authors [*e.g.*, [7,27]]. This parameterization allows us to investigate the behavior of the model regardless of the material characteristics and easily compare its results to those of other models.

$$\tau = \frac{h(t)}{R} \tag{15}$$

$$\nu_V = \frac{4\pi}{3} N_V R^3 \tag{16}$$

$$\nu_S = 4\pi N_S R^2 \tag{17}$$

Where τ is the reduced time, ν_V is the average number of nuclei in the interior of the spherical particles, and ν_S is the average number of nuclei on their surfaces. With this parameterization, Eq. (14) becomes:

$$\alpha^{S,V}(\tau) = 1 - \left\{1 - \left[1 - (1-\tau)^3\right] \cdot \left[1 - \exp\left(-\frac{\nu_S}{4} \cdot \tau^2\right)\right] \times \right\} \cdot \left\{\exp\left(-\nu_V \cdot \tau^3\right)\right\} \tag{18}$$

which is valid for $0 \le \tau \le 1$. As discussed previously, for $\tau > 1$ we make $\tau = 1$ only for the first term of Eq. (18), resulting in Eq. (19).

$$\alpha^{S,V}(\tau) = 1 - \exp\left(-\frac{\nu_S}{4} \cdot \tau^2\right) \cdot \exp\left(-\nu_V \cdot \tau^3\right), \ \tau > 1 \tag{19}$$

It is interesting to note that Equations (18) and (19) do not explicitly depend on particle size. The influences of surface and

internal transformation depend only on their respective number of nucleation sites. In most cases, larger particles should have more nuclei.

Fig. 8 shows simulated curves in terms of the nondimensional parameters, Eq. (18). We clearly see the effect of increasing the number of surface nuclei in Fig. 8 (a). For less than approximately 10 nuclei, full transformation is not achieved when the surface crystals reach the particle center. As the transformed surface regions impinge and the transition from 3D to 1D growth takes place, the curves coincide with the curve for an infinite number of nuclei (dashed curve). In Fig. 8 (b) we see the effect of internal nuclei on a sample with infinite ν_S. As the volumetric transformation takes place, the other curves deviate from the full layer (dashed) curve. In Fig. 8 (c), the effect of both surface and volumetric transformation is shown for a fixed number of 10 surface sites.

4.3. Comparison with other models

4.3.1. Influence of the new surface phase shape: truncated conical vs. semi-spherical

In this section we compare our model with two exact models for surface transformation from a fixed number of nucleation sites. The main difference between these models is that in ours, the new phase grows from the surface with the truncated cone geometry, whereas in the Weinberg [12] and Villa-Rios [13] models, the new phase grows with semispherical geometries. Both exact models can be described by the same parameterized expression, Eq. (20), for $0 \le \tau \le 1$. Villa and Rios' model can be used to calculate the transformation for $1 \le \tau < 2$, and for $\tau \ge 2$ with other equations, not shown here. The reader can refer to the original reference [13] for the unparameterized equations for $1 \le \tau < 2$ and $\tau \ge 2$.

$$\alpha^S(\tau) = 1 - (1-\tau)^3 - 3\int_{1-\tau}^{1} \exp\left(-\frac{\nu_S}{4}\left(2 - \lambda + \frac{1-\tau^2}{\lambda}\right)\right)\lambda^2 d\lambda \tag{20}$$

The models lead to very similar predictions for values of $\nu_S \sim 10$ or higher (Fig. 9). For a given radius, the truncated cones initially have a larger volume than the semi-spheres, but the opposite happens after a certain size. For a single nucleus, this happens at approximately $\tau = 0.6$, *i.e.*, when the crystal reaches about 60% of the particle's radius.

For $\nu_S = 1$, an *average* of a single nucleus per particle, the results differ. For $\tau > 1$, The rigorous equation of Villa & Rios predicts a higher transformed fraction than ours and for $\tau = 2$ the transformation stops for their model. This happens as the transformed region has a radius equal to the particle's diameter and, therefore, no further transformation can take place. Our approximation is not so rigorous, and the particles' surfaces are considered to be occupied following a JMAK equation, for an infinite surface. The volumetric transformed fraction tends to 1 at infinite time, following the surface 2D transformation.

Although this is unrealistic for isolated particles, disregarding the finite sample size may be advantageous for simulating transformations which start in grain boundaries. For instance, in sinter-crystallization of glass particles, as densification progresses, the particles fuse together and the crystals may indeed grow outside them towards the neighbor particle. Surface crystals usually grow onto neighbor coalesced particles, effectively acting as two nucleation sites, which is seen in the micrographs of Ferreira et al. [8,27]. Incomplete densification, which is a common situation for sintered glasses and for particles after a DSC run to high temperatures, probably behaves in between the isolated particle and the fully sintered cases.

4.3.2. Simultaneous surface and internal transformation

The Villa-Rios model for simultaneous surface and bulk transformation is presented in Equation (21), after our parameterization, for $0 \le \tau < 1$. The reader can refer to the original reference [13] for the unparameterized equations for $1 \le \tau < 2$ and $\tau \ge 2$.

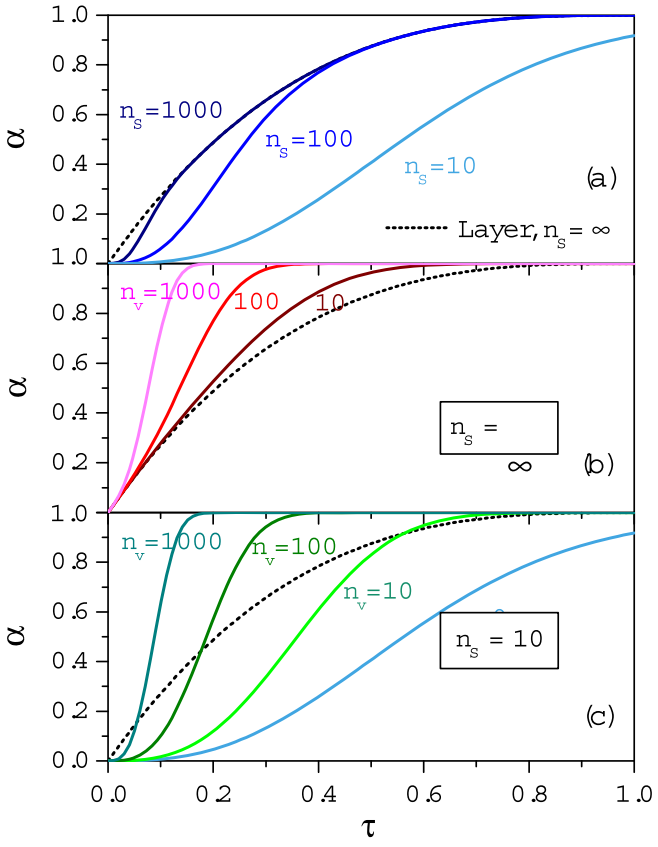

Fig. 8. General transformation curves for: (a) surface transformation, (b) surface (full layer) + volume and (c) surface + volume ($\nu_S = 10$).

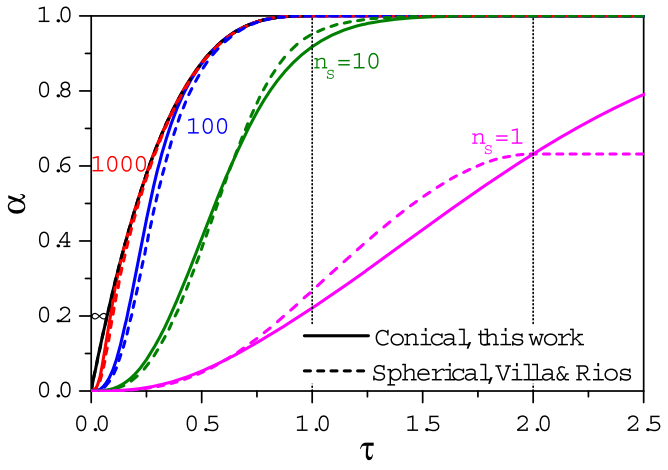

Fig. 9. Influence of crystal shape on surface transformation kinetics. Conical (our model) versus spherical (Weinberg and Villa-Rios models [12,13]) crystals.

$$\alpha^S(\tau) = 1 - (1-\tau)^3 - 3\int_{1-\tau}^{1} \exp\left(-\frac{\nu_S}{4}\left(2 - \lambda + \frac{1-\tau^2}{\lambda}\right)\right)\lambda^2 d\lambda$$

$$\alpha^V(\tau) = 1 - (1-\tau)^3 \exp\left(-\nu_V \tau^3\right) - 3\int_{1-\tau}^{1} \exp(-\nu_V \cdot \rho(\tau,\lambda))\lambda^2 d\lambda$$

$$\rho(\tau) = \frac{1}{16}\left(-\frac{3\tau^4}{\lambda} + 8\tau^3 + \frac{6\tau^2}{\lambda} - 6\tau^2\lambda - \frac{3}{\lambda} + 8 - 6\lambda + \lambda^3\right)$$

$$\alpha^{S,V}(\tau) = 1 - \left(1 - \alpha^S(\tau)\right)\left(1 - \alpha^V(\tau)\right) \quad (21)$$

The results from the models are similar for the simulated conditions, with our model predicting somewhat higher transformed fractions for lower ν_V (Fig. 10). The two main differences between the two models are: (i) the shape of surface transformation, as discussed in the previous section, and (ii) the finite sample size effect. In the Villa-Rios model, the volumetric transformation is limited to the nuclei contained within each particle, while we simply use a JMAK expression for an infinite medium, resulting in the higher transformed fraction seen in Fig. 10. The disregard for finite sample size may be a better approach when applying the model to transformations that start simultaneously from grain boundaries and internal sites, such as glass sintering.

4.3.3. The equation of Levine et al. for internal transformation

As presented in Section 3.1.2, the result of Levine et al. [7], Eq. (11) using $m = 1$, is a good approximation for $\alpha^V(\tau)$ of Eq. (21), for $0 \le \tau < 2$ and an *average* number of crystals per particle. Fig. 11 shows a comparison between the Levine et al. and Villa-Rios models. The maximum difference between the two models is less than 3%.

Finally, different experimental conditions can be modeled by using different combinations of equations for surface and internal transformation. The effect of finite particle size can be disregarded or accounted for, depending on whether the particles sinter during heat treatment. We could also extend the model to a situation where the number of nuclei depends on a constant nucleation rate.

5. Conclusions

We proposed and tested a new, simple model for the kinetics of phase transformations of particles, starting from surface and internal nucleation sites. Our simulations described the crystallization of diopside glass particles very well for different numbers of surface nucleation sites and the simultaneous surface and bulk crystallization of lithium disilicate glass particles.

Our model also compares well with two rigorous (but complex) models of phase transformations. The difference between the models is the shape of the transformed regions from surface sites and that ours relaxes the assumption of finite sample size, considering that crystals from one particle may indeed grow towards other particles (due to sintering). Therefore, the current model may be even more realistic when applied to transformations that start from grain boundaries, such as sintering and DSC experiments with glass particles.

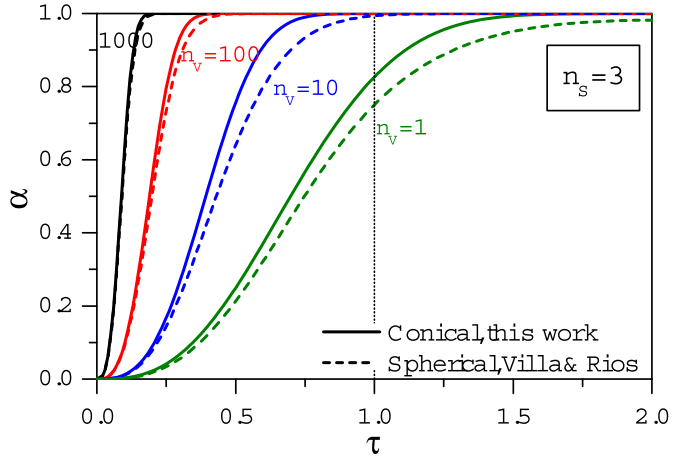

Fig. 10. Simulation results of the current model and the Villa-Rios model [13] for simultaneous surface and bulk transformation. $\nu_S = 3$ for all the curves.

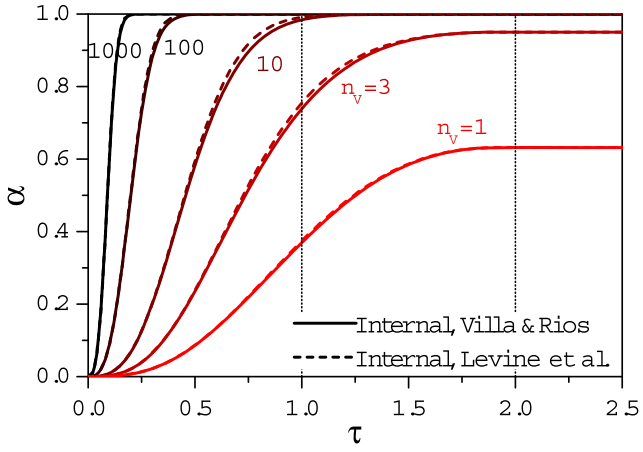

Fig. 11. Levine et al. [7] and Villa-Rios [13] models for particle transformation from an average number of internal nuclei, ν_V.

Acknowledgements

This work was supported by the São Paulo Research Foundation, Fapesp (grant # 2013/07793-6) and the Brazilian National Council of Technological and Scientific Development, CNPq (grant # 143040/2008-1). We thank Dr. Luciana Ghussn for the critical suggestions and discussion of this paper. We also thank Dr. Gregory Rohrer (editor) and the two anonymous reviewers for their comments, which significantly improved this paper.

References

[1] W.A. Johnson, R.F. Mehl, Reaction kinetics in processes of nucleation and growth, Trans. Am. Inst. Min. Metall. Eng 135 (1939) 416–442.

[2] M. Avrami, Kinetics of phase change. I: general theory, J. Chem. Phys. 7 (1939) 1103–1112. https://doi.org/10.1063/1.1750380.

[3] M. Avrami, Kinetics of phase change. II: transformation time relations for random distribution of nuclei, J. Chem. Phys. 8 (1940) 212–224. https://doi.org/10.1063/1.1750631.

[4] M. Avrami, Granulation, phase change, and microstructure: kinetics of phase change. III, J. Chem. Phys. 9 (1941) 177–184. https://doi.org/10.1063/1.1750872.

[5] A.N. Kolmogorov, On the statistical theory of metal crystallization, Izv. Akad. Nauk SSSR Ser Mat 3 (1937) 355–360 (in Russian).

[6] M.C. Weinberg, D.P. Birnie III, V.A. Shneidman, Crystallization kinetics and the JMAK equation, J. Non-cryst. Solids 219 (1997) 89–99. https://doi.org/10.1016/S0022-3093(97)00261-5.

[7] L.E. Levine, K. Lakshmi Narayan, K.F. Kelton, Finite size corrections for the johnson–mehl–avrami–Kolmogorov equation, J. Mater. Res. 12 (1) (1997) 124–132. https://doi.org/10.1557/JMR.1997.0020.

[8] E.B. Ferreira, M.L.F. Nascimento, H. Stoppa, E.D. Zanotto, Methods to estimate the number of surface nucleation sites on glass particles, Phys. Chem. Glasses: Eur. J. Glass Sci. Technol. B 49 (2) (2008) 81–89.

[9] I. Gutzow, R. Pascova, A. Karamanov, J. Schmelzer, The kinetics of surface induced sinter crystallization and the formation of glass ceramic materials,

J. Mater. Sci. 33 (1998) 5265–5273. https://doi.org/10.1023/A:1004400508154.
[10] W. Höland, G.H. Beall, Glass-ceramic Technology, second ed., John Wiley & Sons, Hoboken, 2012.
[11] R. Müller, The influence of grain size on the overall kinetics of surface-induced glass crystallization, J. Therm. Anal. 35 (1989) 823–835. https://doi.org/10.1007/BF02057238.
[12] M.C. Weinberg, Transformation kinetics of particles with surface and bulk nucleation, J. Non-cryst. Solids 142 (1992) 126–132. https://doi.org/10.1016/S0022-3093(05)80015-8.
[13] E. Villa, P.R. Rios, Transformation kinetics for surface and bulk nucleation, Acta Mater. 58 (2010) 2752–2768. https://doi.org/10.1016/j.actamat.2010.01.012.
[14] V.M. Fokin, A.A. Cabral, R.M.C.V. Reis, M.L.F. Nascimento, E.D. Zanotto, Critical assessment of DTA–DSC methods for the study of nucleation kinetics in glasses, J. Non-cryst. Solids 356 (2010) 358–367. https://doi.org/10.1016/j.jnoncrysol.2009.11.038.
[15] R.M.C.V. Reis, A.J. Barbosa, L. Ghussn, E.B. Ferreira, E.D. Zanotto, Sintering and rounding of irregular glass particles, J. Am. Ceram. Soc. (2018) (under review).
[16] W.S. Rasband, J. Image, Bethesda: U. S, National Institutes of Health, 1997-2012. http://imagej.nih.gov/ij/.
[17] D.R. Cassar, A.M. Rodrigues, M.L.F. Nascimento, E.D. Zanotto, The diffusion coefficient controlling crystal growth in a silicate glass-former, Int. J. Appl. Glass Sci. 00 (2017) 1–10. https://doi.org/doi: 10.1111/ijag.12319.
[18] R.M.C.V. Reis, V.M. Fokin, E.D. Zanotto, Determination of crystal growth rates in glasses over a temperature range using a single DSC run, J. Am. Ceram. Soc. 99 (6) (2016) 2001–2008. https://doi.org/doi: 10.1111/jace.14200.
[19] M.L.F. Nascimento, V.M. Fokin, E.D. Zanotto, A.S. Abyzov, Dynamic processes in a silicate liquid from above melting to below the glass transition, J. Chem. Phys. 135 (2011), 194703. https://doi.org/10.1063/1.3656696.
[20] R. Müller, E.D. Zanotto, V.M. Fokin, Surface crystallization of silicate glasses: nucleation sites and kinetics, J. Non-cryst. Solids 274 (2000) 208–231. https://doi.org/10.1016/S0022-3093(00)00214-3.
[21] M.N. Rahaman, Synthesis of powders, in: Ceramic Processing and Sintering, Marcel Dekker, New York, 1995, pp. 49–124.
[22] J.W. Christian, General introduction, in: The Theory of Transformations in Metals and Alloys, 2002, pp. 1–22. Pergamon, Oxford, 3rd ed.
[23] V.M. Fokin, A.S. Abyzov, J.W.P. Schmelzer, E.D. Zanotto, Stress induced pore formation and phase selection in a crystallizing stretched glass, J. Non-cryst. Solids 356 (2010) 1679–1688. https://doi.org/10.1016/j.jnoncrysol.2010.06.008.
[24] J. Šesták, P. Holba, Heat inertia and temperature gradient in the treatment of DTA peaks: existing on every occasion of real measurements but until now omitted, J. Therm. Anal. Calorim. 113 (2013) 1633–1643. https://doi.org/10.1007/s10973-013-3025-3.
[25] M. Raimo, Kinetics of phase transformation of indium in the presence of polytetrafluoroethylene: implications for DSC measurements on polymers and their composites, Int. J. Polym. Sci. 2015 (2015) 9, 690718, https://doi.org/10.1155/2015/690718.
[26] V.M. Fokin, E.D. Zanotto, N.S. Yuritsyn, J.W.P. Schmelzer, Homogeneous crystal nucleation in silicate glasses: a 40 years perspective, J. Non-cryst. Solids 352 (2006) 2681–2714. https://doi.org/10.1016/j.jnoncrysol.2006.02.074.
[27] E.B. Ferreira, V. Lopez-Richard, E.D. Zanotto, G.E. Marques, Analytical model for heterogeneous crystallization kinetics of spherical glass particles, J. Am. Ceram. Soc. 92 (11) (2009) 2616–2618. https://doi.org/10.1111/j.1551-2916.2009.03288.x.s.